Check for updates

Investigations on Convective Heat Transfer Enhancement in Circular Tube Radiator Using Al_2O_3 and CuO Nanofluids

Sobin Alosious
Department of Applied Mechanics,
Indian Institute of Technology,
Chennai 600036, India

S. R. Sarath
Department of Mechanical Engineering,
College of Engineering, Trivandrum,
Thiruvananthapuram 695016, India

Anjan R. Nair
Department of Mechanical Engineering,
College of Engineering, Trivandrum,
Thiruvananthapuram 695016, India
e-mail: anjanrn@gmail.com

K. Krishnakumar
Department of Mechanical Engineering,
College of Engineering, Trivandrum,
Thiruvananthapuram 695016, India

In this study, forced convective heat transfer inside a circular tube automobile radiator is experimentally and numerically investigated. The investigation is carried out using Al_2O_3 and CuO nanofluids with water as their base fluid. A single radiator circular tube with the same dimensions is numerically modeled. Numerical model is validated using the experimental study results. In the experimental study, Al_2O_3 and CuO nanofluids of 0.05% volume concentrations (ϕ) were recirculated through the radiator for the Reynolds number (Re) between 260 and 1560. The numerical investigation is conducted for the nanoparticle volume concentration from 0% to 6.0% and $260 < Re < 1560$. The investigation shows an enhancement of convective heat transfer coefficient (h) with the increase in nanoparticle volume concentration and with the Reynolds number. A maximum enhancement of 38% and 33% were found for Al_2O_3 and CuO nanofluids of $\phi = 1\%$ and $Re = 1560$. For the same cooling load of the radiator, the pumping power can be reduced by 8% and 10%, when Al_2O_3 and CuO nanofluids ($\phi = 0.8\%$) were used. Enhancement in convective heat transfer can be utilized to reduce the radiator surface area required. However, the addition of nanofluid results in an enhancement of density (ρ) and viscosity (μ) along with a reduction in specific heat capacity (C_p). Hence, the selection of nanoparticle volume concentration should consider its effect on the thermophysical properties mentioned earlier. It is found that the preferred concentration is between 0.4% and 0.8% for both Al_2O_3 and CuO nanofluids. In our investigations, it is observed that the convective heat transfer performance of Al_2O_3 nanofluid is better than the CuO nanofluid. [DOI: 10.1115/1.4039924]

Keywords: Al_2O_3, automotive radiator, convective heat transfer, CuO, nanofluids, particle volume concentration, round tube

1 Introduction

Heat transfer in the radiator takes place by three ways. The convective heat transfer between coolant and the radiator tubes inner surface (inside convective heat transfer) followed by the conductive heat transfer across the radiator tubes and then the convective heat transfer between the outer surface of radiator and the air flows outside. Thus, the effective way to improve the radiator efficiency is by the improvement in efficiency of the conductive or convective heat transfers mentioned earlier. Conductive heat transfer depends on the radiator tube material, while the convective heat transfer depends on the temperature difference between the mediums, area of heat transfer, and the convective heat transfer coefficient value (h). Convective heat transfer coefficient (h) between the inside tube surface and the coolant fluid depends on the coolant flow rate and the fluid properties. Due to obvious limitations in increasing the coolant velocity, the best way to improve h value is by changing the coolant used or improve its thermal properties.

Thermal conductivity (k) of coolants influences the convective heat transfer coefficient value (h). k of commonly used coolants like water (H_2O) and ethylene glycol are very less (0.6 and 0.25 W/m-k, respectively). Evolution of nanotechnology leads to the concept of nanofluids, which is a two-phase fluid with solid phase (nanoparticles) as well as liquid phase (base fluid). Nanofluids are fluids that contain suspended nanoparticles of average size less than 100 nm. Ultrafine particles of Al_2O_3, CuO, SiO_2, and TiO_2 have been dispersed in the base fluids. Metallic oxide nanoparticles possess higher thermal conductivity along with stability in the nanofluids. All physical mechanisms have a critical length scale, below which the physical properties of materials are changed. Metallic oxide nanoparticles behave like a fluid molecule in their nanoscale. Therefore, particles less than 100 nm in diameter exhibit properties different from those of conventional solids [1–4]. Stability enhancement of these nanoparticles within the nanofluid is achieved by the addition of chemicals called surfactants such as sodium dodecyl benzene sulphate [5]. Enhancement in heat transfer properties of nanofluids is attributed to the considerable improvement in thermal conductivity of the fluid by the addition of metallic nanoparticles.

A numerical study in an automotive diesel engine flat tube radiator using CuO/H_2O nanofluid with 20 nm particle size and 0–2% particle volume concentration (ϕ) under turbulent flow conditions shows an enhancement of 10% in h and 23.8% in pumping power for the Reynolds number 6000 [6]. Increase in heat transfer efficiency of the radiator influences its design. Thus, using nanofluid coolants with improved heat transfer performance under the required working temperature, the size of the radiator required can be reduced. This keeps the car frontal area more compact and provides scope for new design [7]. A computational fluid dynamics study on a flat tube radiator using Al_2O_3 and CuO nanofluids (base fluid is the mixture of ethylene glycol and water) for the Reynolds number varies from 100 to 2000 shows a maximum enhancement of 94% and 89% for Al_2O_3 and CuO nanofluids,

Contributed by the Heat Transfer Division of ASME for publication in the Journal of Thermal Science and Engineering Applications. Manuscript received July 21, 2017; final manuscript received March 6, 2018; published online May 22, 2018. Assoc. Editor: Amir Jokar.

Copyright © 2018 by ASME

http://thermalscienceapplication.asmedigitalcollection.asme.org/article-pdf/10/5/051012/6338855/tsea_010_05_051012.pdf?casa_token=0vUaYhkudLcAAAAA:e8XZmLYiYsOaRntV47gJLXGOLwdTkv-n4K4Z8yfJGCYCYSYpeTJ3cJuoMXPHVjwVuDOG8Q by University Of Not

respectively, for the concentrations of 10% and 6%. Skin friction value increases with the increase in ϕ and increments the pumping power. But, the increment in h value reduces the amount of nanofluid requires to be pumped for the same radiator cooling load, which eventually reduces the pumping power to 82% and 77% for Al_2O_3 and CuO nanofluids [8]. An experimental study of heat transfer enhancement using water/ethylene glycol based nanofluids in a radiator with Al_2O_3 nanofluid and flow rates from 2 to 6 l/m shows a maximum enhancement of 40% in h for the highest flow rate. The enhancement in convective heat transfer reduces the radiator size and improves the fuel economy [9]. A numerical analysis on convective heat transfer of Al_2O_3/H_2O nanofluids in a single circular tube was done. The study was carried out under laminar developing flow conditions by varying the volume concentrations (ϕ) from 0% to 0.6%. It is found that, increasing the volume concentration causes an increase in fluid pressure drop, which leads to an increase in pumping power. Increment in convective heat transfer performance reduces the amount of fluid flow requires for the same radiator cooling load. Hence, the increment in convective heat transfer was compared with the pumping power change and the optimum volume concentration was found [10].

The present study is the investigation on convective heat transfer (inner side) along with the other flow aspects, such as wall shear stress (τ), Chilton–Colburn factor (j) and pumping power ratio (P_{ratio}) for circular tube radiator. The study is conducted using Al_2O_3/H_2O and CuO/H_2O nanofluids for the Reynolds number between 260 and 1560. A single radiator round tube of the same dimensions is numerically modeled and validated by the results obtained from the experimental test conducted with 0.05% ϕ, Al_2O_3/H_2O and CuO/H_2O nanofluids. This model is used for the further numerical investigation and the studies were conducted for nanoparticle volume concentrations which vary from 0% to 6%. The study explores the role of working conditions such as volume concentration (ϕ) of nanofluid on the heat transfer parameters.

2 Numerical Method

The numerical study was conducted in one of the 35 tubes of the round tube radiator. A single round tube radiator with exact dimensions was modeled. The effects of fins and the radiator thickness were considered by providing proper boundary conditions, which were found out from experimental study. The numerical study was conducted for higher nanofluid concentrations which were not feasible in the experimental study. The numerical study was conducted in ANSYS FLUENT (2015).

2.1 Problem Geometry. The numerical study was carried out on a single round tube of the radiator. Round tube is of circular cross section with the diameter of 6.4 mm, length of 310 mm and thickness of 0.35 mm. Geometry of the round tube is shown in the Fig. 1.

2.2 Governing Equations. Nanoparticle concentration is very low in the nanofluid hence it is assumed as a single phase fluid. The nanofluid is considered as incompressible and Newtonian fluid. The heat dissipation due to viscous effect and radiative effect are not accounted. The continuity, momentum, and energy equations were solved in three-dimensional Cartesian coordinates under the aforementioned assumptions using ANSYS FLUENT (2015).

2.2.1 Continuity Equations. The continuity equation for the flow of nanofluid is given by

$$(\nabla.\bar{V}) = 0 \tag{1}$$

2.2.2 Momentum Equations. The momentum equation for the flow of nanofluid is given by

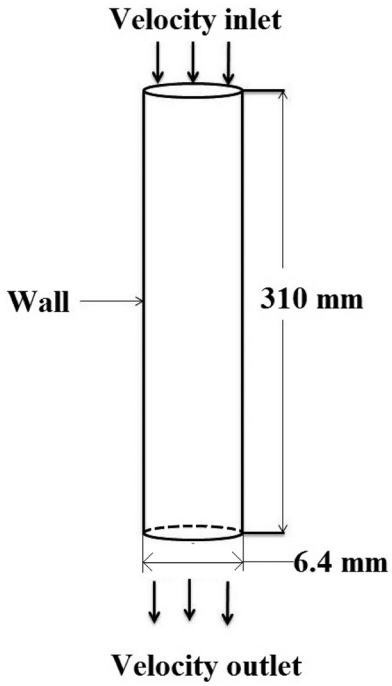


Fig. 1 Geometry and dimensions of circular tube

$$\rho(\nabla.\bar{V})\bar{V} = -\nabla P + \mu\nabla^2\bar{V} \tag{2}$$

2.2.3 Energy Equations. The energy equation for the flow of nanofluid is given by

$$\rho C_p(\nabla.\bar{V})T = \nabla^2(kT) \tag{3}$$

2.3 Boundary Conditions. The boundary conditions used for solving the continuity, momentum, and energy equations are as follows:

The inlet of the round tube is subjected to a constant temperature and axial velocity ($u = v = 0$, $w = w_\infty$). The inlet velocity is varying according to different Reynolds numbers. The inlet temperature is 90 °C, which is the temperature of coolant coming out of the engine coolant jacket. The flow is of developing type hence, at the outlet of the round tube pressure outlet boundary condition is used with zero gauge pressure ($P = P_{atm}$). No-slip boundary condition is provided at the wall of radiator tube for velocity ($u = v = w = 0$). The thermal boundary condition is of convective heat transfer, the outside heat transfer coefficient is taken from the experimental analysis (Eq. (15)). The outlet free stream air temperature is considered as constant.

2.4 Numerical Computation. The governing equations [1–3] were solved using the aforementioned boundary conditions by control volume approach in ANSYS FLUENT 15. The scheme used in this analysis was a staggered grid method such that the velocity components at the control volume faces were calculated and the remaining variables were saved at the central node of the control volume. Semi-implicit methods were used for coupling pressure and velocity. The pressure gradient was calculated using least square cell based interpolation method by calculating the pressure at the cell-face. The pressure terms were discretized using a second-order scheme and the momentum and energy terms were discretized using second-order upwind scheme. The simulations were truncated after the residuals of continuity, momentum, and energy terms reach below 10^{-6}. The simulation data were used for postprocessing.

Downloaded from digitalcollection.asme.org/thermalscienceapplication/article-pdf/10/5/051012/6338855/tsea_010_05_051012.pdf?casa_token=0vUaYhkudLcAAAAA:e8XZmLYiYsOaRntV47gJLXGOLwdTkv-n4K4Z8yfJGCYCYSYpeTJ3cJuoMXPHVjwVuDOG8Q by University Of Not

2.5 Grid Independence Study. The three-dimensional meshing of the geometry was generated by using ICEM CFD, which is a mesh generation program of ANSYS (2015). Cross-sectional view of the mesh is shown in Fig. 2. Four different mesh sizes were chosen (mesh-I, mesh-II, mesh-III, and mesh-IV listed in Table 1) in order to confirm the grid independence. The simulations were carried out for four different sized meshes by keeping the other parameters constant. By comparing the surface weighted average values of velocity and temperatures at the outlet, we have obtained that the results of mesh-I, mesh-II, and mesh-III shows some variation while the results of mesh-III and mesh-IV overlap. Therefore, we have selected mesh-III and used throughout this study, because there is only negligible variation in results even after increasing the grid density.

3 Experimental Method

The experimental analysis is done using water, Al_2O_3/H_2O, and CuO/H_2O nanofluids. Initially both Al_2O_3/H_2O and CuO/H_2O nanofluids with 0.05% volume concentrations were prepared. They were recirculated through the round tube automobile radiator. The temperature of nanofluid is kept constant at 90 °C. The Reynolds number varies from 260 to 1560.

3.1 Preparation of Nanofluid. Nanofluids were prepared by two-step method, in which nanoparticles, nanofibers, nanotubes, or other nanomaterials are first produced and will be dispersed into the base fluid with the help of magnetic force agitation, ultrasonic agitation, or high shear mixing. In this work, both Al_2O_3 and CuO nanoparticles were purchased from Sigma Aldrich Chemicals, Bangalore, India. These nanoparticles were dispersed in de-ionized water using a probe type sonicator and nanofluids of 0.05% were prepared. Before each set of experiments, the nanofluid was ultrasonicated again to ensure full mixing of the nanoparticles and base fluid. After each set of tests, radiator tubes, storage tank, and delivery pipes were flushed and cleaned with distilled de-ionized water. The prepared nanofluids were immediately used for experimental analysis which prevents sedimentation of nanoparticles. These procedures were followed from other experimental studies to obtain a stable nanofluid mixture [11,12]. The properties of CuO and Al_2O_3 nanoparticles required for the calculation of the thermophysical properties of nanofluids are shown in Table 2. Sodium dodecyl benzene sulfate surfactant with 1/4th weight of nanoparticles were added. Surfactants were added to improve the stability of the nanofluid by preventing the sedimentation of the nanoparticles within the base fluid. Volume concentration of nanofluid is calculated by using the following equation:

$$\phi = \left[\frac{(w_{np}/\rho_{np})}{(w_{np}/\rho_{np}) + (w_{bf}/\rho_{bf})}\right] \times 100 \tag{4}$$

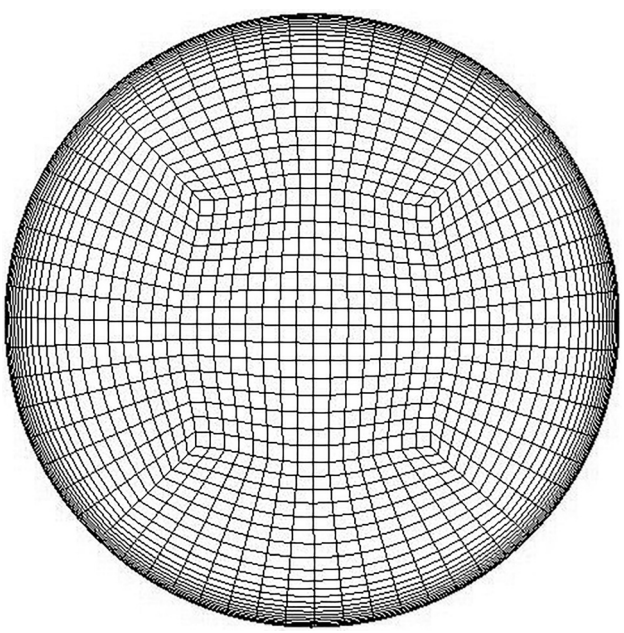


Fig. 2 Cross-sectional view of grid layout used in the present study

Table 1 Surface weighted average temperature and average velocity at the outlet of round tube for four different meshes (The mesh III was selected and used throughout this study)

Grid	Velocity (m/s)	Temperature (K)
Mesh-I (30 × 30 × 50)	0.319939	344.6028
Mesh-II (45 × 45 × 75)	0.319818	344.5614
Mesh-III (50 × 50 × 100)	**0.319762**	**344.5536**
Mesh-IV (55 × 55 × 125)	0.319722	344.5530

3.2 Thermophysical Properties of Nanofluid. The thermophysical properties of nanofluids such as density (ρ), specific heat capacity (C_p), thermal conductivity (k), and viscosity (μ) can be found out by either experimentally or by using correlations. In this study, the nanofluid properties were evaluated by using the following correlations (5–10). The thermophysical properties of nanofluid depend on properties of nanoparticles and base fluid and concentration of nanoparticles.

3.2.1 Specific Heat Capacity and Density. The density and specific heat capacity of nanofluids can be evaluated using physical mixture rule by assuming thermal equilibrium between the base fluid and nanoparticles [13]

$$C_{p,nf} = \frac{\varphi\rho_{np}C_{p,np} + (1-\varphi)\rho_{bf}C_{p,bf}}{\rho_{nf}} \tag{5}$$

The equation for density is given by

$$\rho_{nf} = \varphi\rho_p + (1-\varphi)\rho_{bf} \tag{6}$$

3.2.2 Thermal Conductivity. Thermal conductivity of nanofluids increases due to addition of higher thermal conductivity nanoparticles and due to Brownian motion of nanoparticles in the base fluid [14]. The thermal conductivity of Al_2O_3/H_2O and CuO/H_2O nanofluids can be calculated from the following correlation [15]. This correlation combines static part of Maxwell's theory and the effect of Brownian motion of nanoparticles in base fluid. The effective thermal conductivity of nanofluid depends on thermal conductivity, volume fraction, density, particle size of nanoparticle and thermal conductivity, density, specific heat capacity, and temperature of the base fluid

$$k_{effective} = k_{static} + k_{Brownian} \tag{7}$$

The Maxwell's equation for k_{static} of spherical particles is given by [16]

Table 2 Thermophysical properties of CuO and Al_2O_3 nanoparticles [12]

Nanoparticles/properties	CuO	Al_2O_3
Density	6510 kg/m^3	3970 kg/m^3
Specific heat capacity	540 J/kg K	525 J/kg K
Thermal conductivity	33 W/m K	17.65 W/m K
Purity	99%	99%
Diameter	<50 nm	<50 nm

Downloaded from http://thermalscienceapplication.asmedigitalcollection.asme.org/article-pdf/10/5/051012/6338855/tsea_010_05_051012.pdf?casa_token=0vUaYhkudLcAAAAA:e8XZmLYiYsOaRntV47gJLXGOLwdTkv-n4K4Z8yfJGCYCYSYpeTJ3cJuoMXPHVjwVuDOG8Q by University of Not

$$k_{static} = \frac{k_{np} + 2k_{bf} - 2(k_{bf} - k_{np})\varphi}{k_{np} + 2k_{bf} + (k_{bf} - k_{np})\varphi} k_{bf} \quad (8)$$

The correlation for dynamic part, $k_{Brownian}$ is given by

$$k_{Brownian} = 5 \times 10^4 \beta\varphi\rho_{bf} C_{p,bf} \sqrt{\frac{\kappa T}{\rho_{np} d_{np}}} f(T, \varphi) \quad (9)$$

where correlation for $f(T, \varphi)$ is given by

$$f(T, \varphi) = \left(2.8217 \times 10^{-2}\varphi + 3.917 \times 10^{-3}\right)\frac{T}{T_0} + \left(-3.0669 \times 10^{-2}\varphi - 3.91123 \times 10^{-3}\right)$$

β was estimated experimentally, For Al_2O_3/H_2O nanofluids, $\beta = 8.4407(100\varphi)^{-1.07304}$ and for CuO/H_2O nanofluids, $\beta = 9.881(100\varphi)^{-0.9446}$.

3.2.3 Viscosity. The viscosity of the nanofluid was claculated using Einstein's equation [17]. The Einstein's equation is suitable for spherical inert particles with less than 5.0% volume concentration. The interaction between water and oxide particles are neglected in this study and nanoparticles are assumed to be inert particles in base fluid. De-ionized water is used for reducing the oxide–water interactions. The Einstein's equation is defined as follows:

$$\mu_{nf} = \mu_{bf}(1 + 2.5\varphi) \quad (10)$$

3.3 Experimental Setup. The experimental setup (Fig. 3) consists of a constant temperature bath of 15 l capacity with a heater of 2.5 kW fixed inside it. Nanofluid is kept inside this bath at a temperature of 90 °C (363 K), which is the normal temperature of radiator coolant coming out of the engine jacket. Nanofluid is pumped from the bath to the radiator with a DC centrifugal pump of 150 W capacity. The radiator is fixed inside a duct with a DC fan of 120 W provided to enhance the air flow velocity through the radiator tubes. The radiator is circular tube type and made of Aluminum. There are 35 tubes; each tube has a length of 310 mm length and 6.4 mm diameter. Rotameter is fixed to measure the nanofluid flow rate; the least count is 0.1 l/m. The nanofluid flow rate through the radiator is controlled by ball valves. The temperature of nanofluid inside the bath is controlled by a temperature controller that controls the power supply to the heater coil. Two RTD PT100 sensors are connected to the nanofluid flow lines with an accuracy of ±0.1 °C, one at the inlet of radiator and another one at the outlet of radiator. The air flow velocity as well as temperatures are measured by using Anemometer having 0.1 m/s least count. The surface temperature of the radiator tubes are measured using 6 K-type thermocouples with an accuracy of ±0.1 °C, placed along the outer surface of a radiator tube. The 220 V AC supply was converted to 12 V DC by using a 12 V, 40 A switch-mode power supply for the working of centrifugal pump and cooling fan.

3.4 Calculation of Heat Transfer Parameters. Following steps were used to find out the convective heat transfer coefficient between air and tube outside surface:

According to Newton's law of cooling

$$Q_{air} = h_{out} A_{out} \Delta T = h_{out} A_{out} (T_{b,air} - T_{wall}) \quad (11)$$

where A_{out} is the outside surface area of the radiator tubes with fin areas considered, h_{out} is the outside convective heat transfer coefficient, and $T_{b,air}$ is the bulk air temperature

$$T_{b,air} = \frac{T_{air,inlet} + T_{air,outlet}}{2} \quad (12)$$

T_{wall} is the average surface temperature of the radiator tube wall

$$T_{wall} = \frac{T_1 + T_2 + \cdots + T_6}{6} \quad (13)$$

T_1–T_2 denotes the temperature at different positions of radiator tube wall. Measurement of A_{out} is a difficult task, but it has a strong impact on the h_{out} value. To overcome this difficulty the following procedure was followed:

$$h_{out} A_{out} = Q_{air}/\Delta T \quad (14)$$

A new term h^*_{out} is used which is defined as the outside surface convective heat transfer coefficient with the fin area considered

$$h^*_{out} = h_{out} A_{out}/A_{out,wf} \quad (15)$$

where $A_{out,wf}$ is the area of the radiator tubes with fin area not considered. Heat, transferred to the air from the radiator tube surface is same as the heat carried away by air, which is

$$Q_{air} = \dot{m}_{air} C_{p,air} \Delta T = \dot{m}_{air} C_{p,air} (T_{air,inlet} - T_{air,outlet}) \quad (16)$$

where $\dot{m}_{air}$ is the mass flow rate and $C_{p,air}$ is the specific heat of air. $T_{air,inlet}$ and $T_{air,outlet}$ are inlet and outlet temperature of air in the duct.

The convective heat transfer coefficient between nanofluid and the inside tube surface is found by

$$Q_{nf} = h_{in} A_{in} \Delta T = h_{in} A_{in} (T_{b,nf} - T_{wall}) \quad (17)$$

where A_{in} is the inside surface area of the tube, h_{in} is the inside heat transfer coefficient, and $T_{b,nf}$ is the bulk fluid temperature

$$T_{b,nf} = \frac{T_{nf,inlet} + T_{nf,outlet}}{2} \quad (18)$$

where $T_{nf,inlet}$ and $T_{nf,outlet}$ are inlet and outlet temperature, respectively, and T_{wall} is the wall temperature which is found from Eq. (13).

Heat transfer rate of nanofluid is given by

$$Q_{nf} = \dot{m}_{nf} C_{p,nf} \Delta T = \dot{m}_{nf} C_{p,nf} (T_{nf,inlet} - T_{nf,outlet}) \quad (19)$$

where $\dot{m}_{nf}$ is the mass flow rate and $C_{p,nf}$ is the specific heat of nanofluid.

Tube side Nusselt number is given by

$$Nu_{exp} = \frac{h_{inlet} d_{hyd}}{k_{nf}} \quad (20)$$

where d_{hyd} is the hydraulic mean diameter and k_{nf} is the thermal conductivity of nanofluid.

Reynolds number of nanofluid is given by

$$Re_{nf} = \frac{\rho_{nf} V_{nf} d_{hyd}}{\mu_{nf}} \quad (21)$$

The performance of the heat exchanger is analyzed by the ε-number of transfer units (NTU) technique and the effectiveness ε is defined as

$$\varepsilon = \frac{Q_{avg}}{(\dot{m} C_p)_{min} (T_{nf,inlet} - T_{air,inlet})} \quad (22)$$

where Q_{avg} is given by

$$Q_{avg} = \frac{Q_{nf} + Q_{air}}{2} \quad (23)$$

Downloaded from http://asmedigitalcollection.asme.org/thermalscienceapplication/article-pdf/10/5/051012/6338855/tsea_010_05_051012.pdf?casa_token=0vUaYhkudLcAAAAA:e8XZmLYiYsOaRntV47gJLXGOLwdTkv-n4K4Z8yfJGCYCYSYpeTJ3cJuoMXPHVjwVuDOG8Q by University of Not

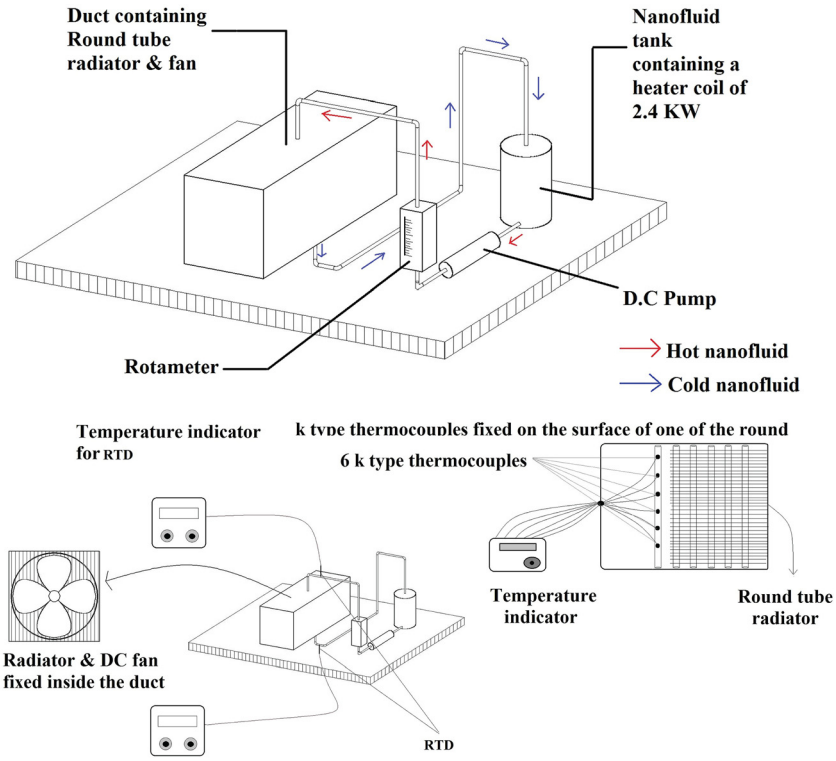


Fig. 3 Schematic diagram of the experimental setup

The relation between effectiveness ε and NTU is given by

$$\varepsilon = \frac{1}{C_r}\left[1 - e^{-C_r(1-e^{NTU})}\right] \tag{24}$$

The capacity ratio C_r is given by

$$C_r = \frac{(\dot{m}C_p)_{min}}{(\dot{m}C_p)_{max}} \tag{25}$$

The overall heat transfer coefficient can be calculated by using the following equation:

$$NTU = \frac{UA}{(\dot{m}C_p)_{min}} \tag{26}$$

The coefficient of friction value f is calculated as

$$f = \frac{\tau}{\frac{1}{2}\rho_{nf}V_{nf}^2} \tag{27}$$

The overall heat transfer coefficient U can also be estimated from the following overall resistances:

$$\frac{1}{UA} = \frac{1}{h_{out}A_{out}} + \frac{t}{k_{wall}A_{wall}} + \frac{1}{h_{in}A_{in}} \tag{28}$$

where h is convection heat transfer coefficient, A is heat transfer surface area, k_t is thermal conductivity of the tube wall, t is the tube wall thickness, and the subscripts out, in, wall denote outside surface, inside surface, and tube wall, respectively.

Chilton–Colburn factor is given by the equation

$$j = \frac{h_{in}}{C_{p,nf}\rho_{nf}V_{nf}}\left(\frac{C_{p,nf}\mu_{nf}}{k_{nf}}\right)^{2/3} \tag{29}$$

The pressure drop in the radiator tube can be evaluated by the following equation:

$$\Delta P = f\frac{4L}{d_{hyd}}\frac{1}{2}\rho V_{nf}^2 \tag{30}$$

where f is the coefficient of friction obtained from computation, L is the length of the tube, and V_{nf} is the velocity of nanofluid through the radiator tubes.

The pumping power can be calculated from the following equation:

$$W = AV_{nf}(\Delta P) \tag{31}$$

where ΔP is the pressure drop across the tube, V_{nf} is the velocity of the nanofluid through the radiator tube, and A is the cross-sectional area of the tube.

The hydrodynamic boundary length (δ_{hl}) is given by the equation

$$\delta_{hl} = 0.05 \times Re \times D \tag{32}$$

The thermal boundary length (δ_{tl}) is given by the equation

$$\delta_{tl} = 0.05 \times Re \times D \times Pr \tag{33}$$

where Pr is the Prandtl number.

3.5 Uncertainty Analysis. Kline–McClintok method [18] was used to calculate the uncertainties in Reynolds number, Nusselt number, and heat transfer coefficient by using uncertainties associated with individual measurements. Uncertainties of fundamental parameters such as flow meter, thermocouples, RTDs, Hot wire anemometer, and pressure gauges were obtained from the manufacturer specifications. Based on the above method, the function R is calculated from "n" independent variables given by

Downloaded from http://thermalscienceapplication.asmedigitalcollection.asme.org/article-pdf/10/5/051012/6338855/tsea_010_05_051012.pdf?casa_token=0vUaYhkudLcAAAAA:e8XZmLYiYsOaRntV47gJLXGOLwdTkv-n4K4Z8yfJGCYCYSYpeTJ3cJuoMXPHVjwVuDOG8Q by University Of Not

$$R = R(x_1, x_2, x_3, \ldots, x_n) \tag{34}$$

Then the uncertainty w_R in the result can be determined by combining uncertainties of individual terms, given by the following equation:

$$w_R = \left[\left(\frac{\partial R}{\partial x_1} w_1\right)^2 + \left(\frac{\partial R}{\partial x_2} w_2\right)^2 + \cdots + \left(\frac{\partial R}{\partial x_n} w_n\right)^2\right]^{1/2} \tag{35}$$

where $w_1, w_2, \ldots, w_n$ are the uncertainties associated with the independent variables $x_1, x_2, \ldots, x_n$, respectively. For Reynolds number, the independent variables' velocity and hydraulic diameter are measured by Roatameter and Vernier caliper with an uncertainty of ± 0.1 l/m and ± 0.02 mm, respectively. The uncertainties in temperature measurement using RTD PT100 and k type thermocouples are $\pm 1\,^{\circ}\mathrm{C}$. The maximum uncertainties of Reynolds number, Nusselt number, effectiveness, inside heat transfer coefficient, and outside heat transfer coefficient are $\pm 3.34\%$, $\pm 3.7\%$, $\pm 3.94\%$, $\pm 3.69\%$, and $\pm 2.81\%$, respectively.

3.6 Validation of Numerical Method. Numerical model was validated with previous works and experimental study results. The experimental studies were conducted by using nanofluids of 0.05% particle volume concentrations for Reynolds numbers varies from 260 to 1560. Figure 4 shows the comparison of the correlation given by Maiga et al. [19], the experimental data of Heris et al. [20] and the numerical results of Manca et al. [10] with the present work for $\phi = 1\%$ of Al_2O_3/H_2O nanofluid. In Fig. 4, it is possible to observe the Nusselt number behavior for $\phi = 1\%$, shows a good agreement with the experimental and numerical results. Moreover, a maximum deviation of about 11%, in the case of $\mathrm{Re} = 1500$, is estimated.

The variation of Nusselt number (Nu) and coefficient of friction (f) with respect to Reynolds number were obtained (Fig. 5). The comparison shows a maximum variation of 10% in Nusselt number and 12% in friction factor.

The validation curves of CuO/H_2O nanofluid with 0.05% particle volume is shown in Fig. 6. The maximum variations in Nusselt number and friction factor are 9% and 13%, respectively.

The variation in Nu for the present numerical results is due the assumptions regarding neglecting the tube thickness resistance and axial conduction through the tube wall. Thus the numerical model is found consistent and used in the further investigations.

4 Results and Discussions

4.1 Variation of Convective Heat Transfer Coefficient and Nusselt Number. Variation in convective heat transfer coefficient (h) with respect to Reynolds number (Re) for Al_2O_3/H_2O nanofluid is shown in Fig. 7. The h increases with the increase in Re and nanoparticle volume concentration (ϕ). A maximum of 38% enhancement is observed for $\phi = 1\%$. A similar trend was noticed for CuO/H_2O nanofluid (Fig. 8), with the maximum enhancement of 33% in h value for $\phi = 1\%$. The enhancement in h is more for Al_2O_3/H_2O nanofluid compared to that of CuO/H_2O nanofluid.

Variation in Nusselt (Nu) with respect to Re for Al_2O_3/H_2O nanofluid with ϕ value ranges from 0% to 1% is shown in Fig. 9. The Nu increases with increase in Re; however, it decreases with increase in ϕ value for the range of 0–1%. A similar trend was noticed for CuO/H_2O nanofluid (Fig. 10). Nu is proportional to h and inversely proportional to thermal conductivity (k) (Eq. (20)), Addition of nanoparticles to the base fluid increases both the k and h. For the ϕ ranges from 0% to 1%, the increment in k predominates the increment in h.

Variation of Nu with respect to Re for Al_2O_3/H_2O nanofluid with ϕ value ranges from 0% to 6% is shown Fig. 11. Nu is decreases with the increment in ϕ up to 1% and then increases from 2% to 6%. A similar trend was noticed for CuO/H_2O nanofluid (Fig. 12). For the ϕ ranges from 2% to 6%, the increment in h predominates the increment in k. A maximum enhancement of 11% and 12% of Nu is observed for Al_2O_3/H_2O and CuO/H_2O nanofluids for $\phi = 6\%$.

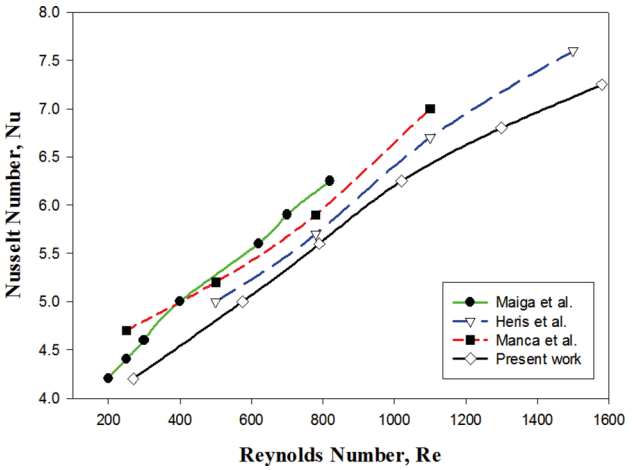


Fig. 4 Comparison of numerical study results of Al_2O_3/H_2O nanofluid with previous works

Thermal boundary layer thickness (δ_t) reduces with the increase in Re (Fig. 13). This reduction in δ_t is the reason for enhancement in h with the increment in Re (Figs. 7 and 8).

4.2 Variation of Wall Shear Stress and Chilton–Colburn Factor. The variation of average wall shear stress ratio of nanofluid to base fluid (τ/τ_{water}) of a single round tube radiator with respect to nanoparticle volume concentration (ϕ) is plotted in Fig. 14. A constant velocity of 0.089 m/s (corresponds to the Reynolds number of 1560 for water) is taken for all the analysis. Wall shear stress increases with increase in ϕ, though the increment is more for Cuo/H_2O nanofluid than that of Al_2O_3/H_2O nanofluid. A maximum enhancement of 3% and 2.5% were observed for Cuo/H_2O and Al_2O_3/H_2O nanofluids for $\phi = 1.0\%$. The increment in τ is an undesirable effect of nanofluid, which is found more when the Cuo/H_2O nanofluid is used. The wall shear stress (τ) directly affects the coefficient of friction (f) (Eq. (27)). The increment in f causes more pressure drop (Eq. (30)) and hence the pumping power of nanofluid.

Figure 15 shows the variation of Chilton–Colburn factor (j) with respect to ϕ for a $\mathrm{Re} = 1560$. Chilton–Colburn factor represents enhancement in the convective heat transfer along with the frictional losses. Chilton–Colburn factor increases with the increase in nanoparticle volume concentration up to $\phi = 0.4\%$.

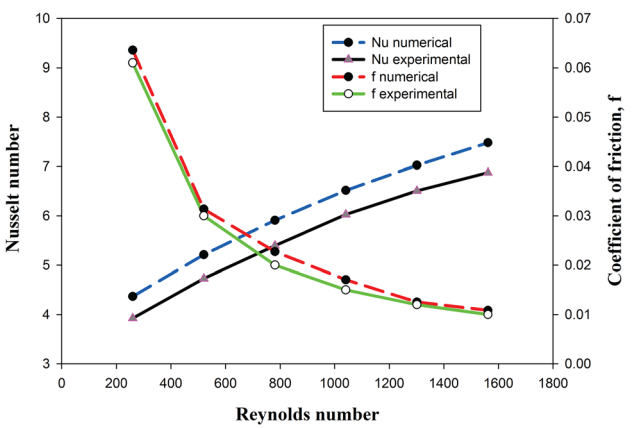


Fig. 5 Comparison of experimental and numerical study results of Al_2O_3/H_2O nanofluid with 0.05% particle volume concentration

Digital Collection. asme.org/thermalscienceapplication/article-pdf/10/5/051012/6338855/tsea_010_05_051012.pdf?casa_token=0vUaYhkudLcAAAAA:e8XZmLYiYsOaRntV47gJLXGOLwdTkv-n4K4Z8yfJGCYCYSYpeTJ3cJuoMXPHVjwVuDOG8Q by University Of Not

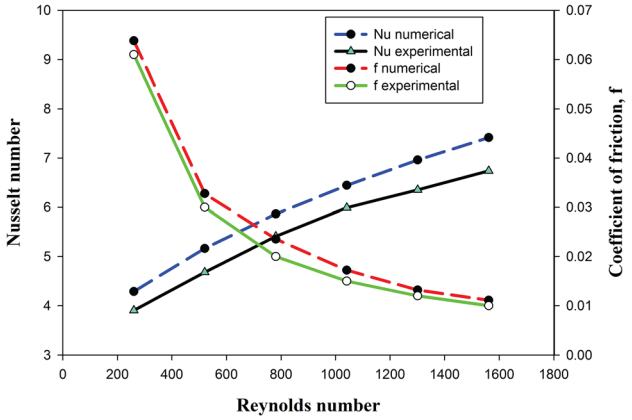


Fig. 6 Comparison of experimental and numerical study results of CuO/H_2O nanofluid with 0.05% particle volume concentration

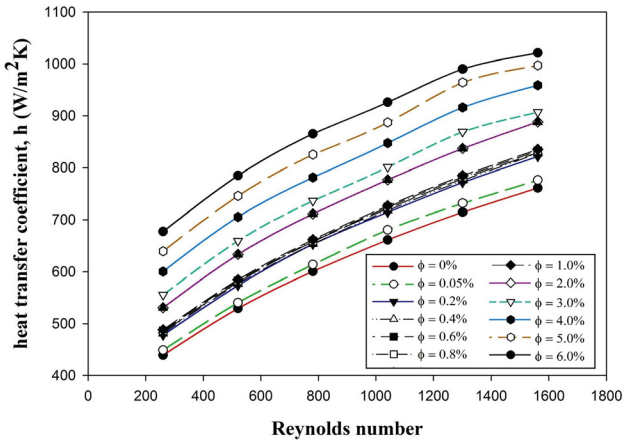


Fig. 8 Variation of convective heat transfer coefficient with respect to Reynolds number for CuO/H_2O nanofluid

However, for higher concentrations, the variation is negligible. Up to $\phi = 0.4\%$, the increment in convective heat transfer predominates the increment in frictional losses and beyond that the increment in frictional losses predominates the enhancement in convective heat transfer.

4.3 Variation of Convective Heat Transfer Coefficient and Wall Shear Stress Along the Length of the Tube. The variation of local convective heat transfer coefficient (h_{local}) along the length of the tube is shown in Fig. 16. It decreases along the length. Local convective heat transfer coefficient at a given length of the tube is highest for Al_2O_3/H_2O nanofluid compared to Cuo/H_2O nanofluid and water. The reason for the variation in h_{local} is explained by the variation of local wall shear stress (τ_{local}) along the length of the tube (Fig. 17).

The local wall shear (τ_{local}) decreases along the length of the tube. CuO/H_2O nanofluid has more τ_{local} than that of Al_2O_3/H_2O nanofluid. The τ_{local} is proportional to the velocity gradient, hence the reduction in τ_{local} is because of the reduction in velocity gradient which is due to the boundary layer formation. The thickness of boundary layer has increased from inlet to outlet of the tube. The entire tube length (0.31 m) is in the hydrodynamic developing region (Eq. (32)); the thermal boundary layer is also in the developing region (Eq. (33)).

4.4 Variation of Pumping Power Ratio and Area Ratio. Addition of nanoparticles enhances the thermophysical properties of coolant fluids. With the same radiator dimensions followed, the nanofluid flow velocity (V_{nf}) required is lesser than that of water to achieve the same cooling load (surface heat transfer flux). The pumping power value (Eq. (31)) depends on flow velocity and

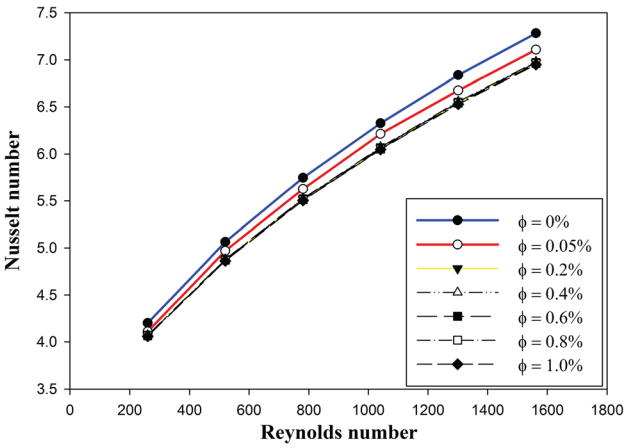


Fig. 9 Variation of Nusselt number with respect to Reynolds number for Al_2O_3/H_2O nanofluid ($0 < \phi < 1.0\%$)

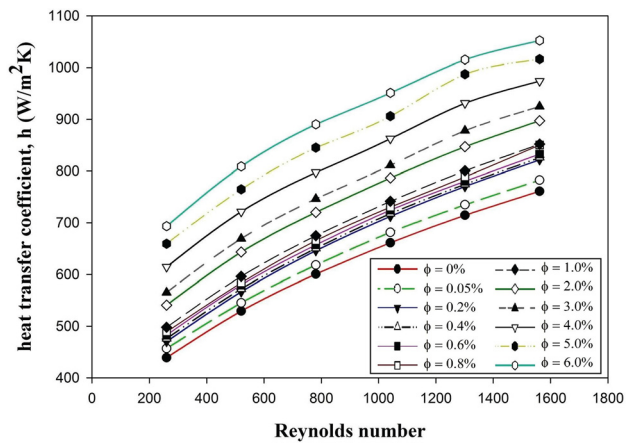


Fig. 7 Variation of convective heat transfer coefficient with respect to Reynolds number for Al_2O_3/H_2O nanofluid

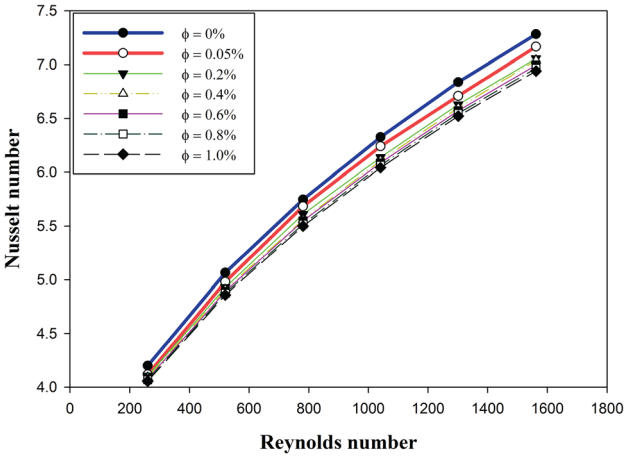


Fig. 10 Variation of Nusselt number with respect to Reynolds numbers for CuO/H_2O nanofluid ($0 < \phi < 1.0\%$)

Digitalcollection.asme.org/thermalscienceapplication/article-pdf/10/5/051012/6338855/tsea_010_05_051012.pdf?casa_token=0vUaYhkudLcAAAAA:e8XZmLYiYsOaRntV47gJLXGOLwdTkv-n4K4Z8yfJGCYCYSYpeTJ3cJuoMXPHVjwVuDOG8Q by University Of Not

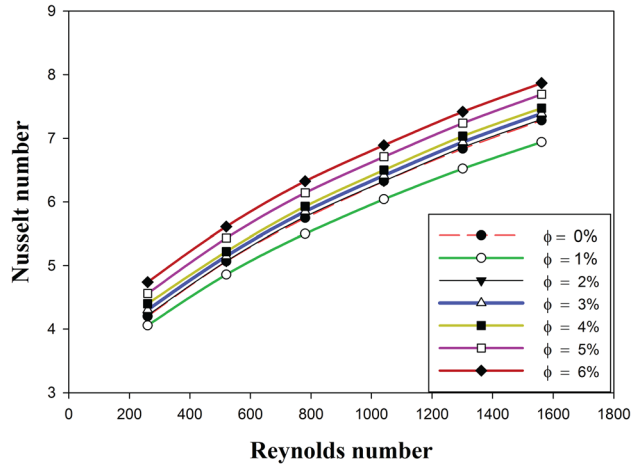


Fig. 11 Variation of Nusselt number with respect to Reynolds numbers for Al_2O_3/H_2O nanofluid ($0 < \phi < 6.0\%$)

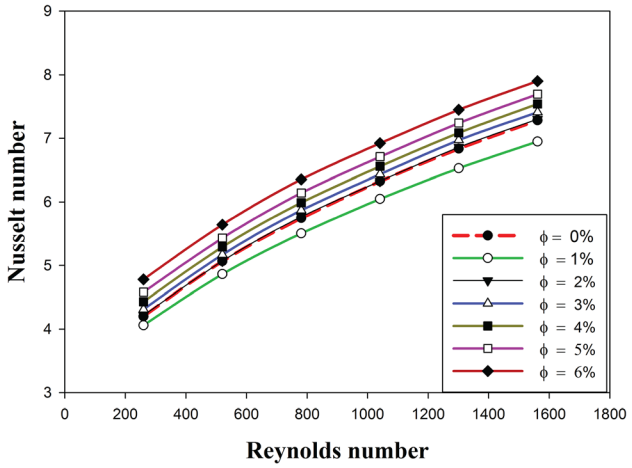


Fig. 12 Variation of Nusselt number with respect to Reynolds numbers for CuO/H_2O nanofluid ($0 < \phi < 6.0\%$)

the pressure drop (ΔP). The pressure drop value is increased by the addition of nanoparticles. Thus, the term pumping power ratio (P_{ratio}) is obtained, which is defined as the ratio of pumping power required with nanofluid to the pumping power required with water. Enhancement in convective heat transfer performance of the nanofluid can be utilized to reduce the radiator surface area required to achieve the same cooling load. The term, area ratio (A_{ratio}) is obtained. It is defined as the ratio of surface area of radiator required with nanofluid to the surface area required with water.

For both Al_2O_3 and CuO nanofluids the P_{ratio} decreases with increase in nanoparticle volume concentration (ϕ) from 0% to 0.8% (Figs. 18 and 19). Interestingly, P_{ratio} increases beyond 0.8%. The reduction in nanofluid flow velocity predominates the increment in pressure drop up to 0.8%, and thus, the pumping power required is reduced. A maximum reduction of 8% in P_{ratio} is observed for both Al_2O_3/H_2O and CuO/H_2O nanofluids. The A_{ratio} value decreases with increase in ϕ. For the same Reynolds number, the convective heat transfer flux increases with increase in nanoparticle volume concentration; thus, the area required for the convective heat transfer reduces (total convective heat transfer rate (W) = heat transfer flux (W/m^2) × area of radiator (m^2)).

Table 3 shows the comparison of pumping power reduction and area reduction of present work with Ray and coworkers [15]. The difference in pumping power and area reduction for both the works are due to the differences in Reynolds number and dissimilar base fluids. Ray and coworkers used Ethylene Glycol/Water (EG/W) as the base fluid and the Reynolds number corresponding to this result is 235. But, in the present study, the base fluid is water and Reynolds number corresponding to this result is 1560.

4.5 Variation of (Convective Heat Transfer Ratio × Specific Heat Capacity Ratio) Factor and Influence Factor. Increment in nanoparticle volume concentration (ϕ) triggers an

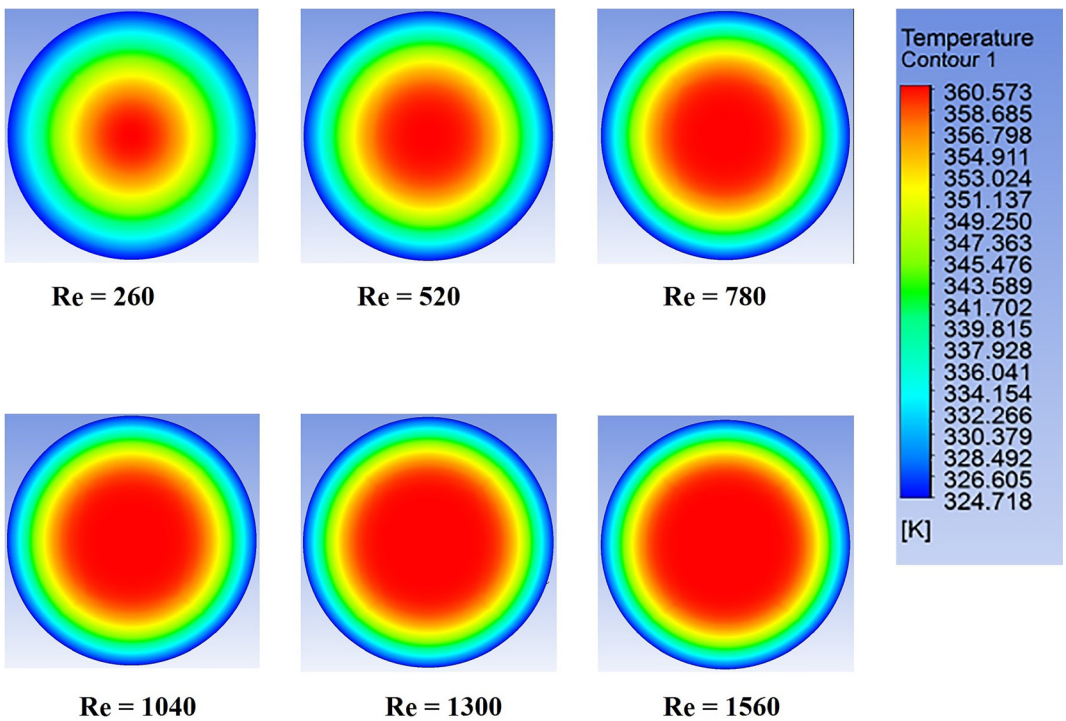


Fig. 13 Variation of Al_2O_3/H_2O nanofluid temperature at the outlet cross section of the tube for six different Reynolds numbers, $\phi = 1.0\%$

Downloaded from thermalscienceapplication.asmedigitalcollection.asme.org/article-pdf/10/5/051012/6338855/tsea_010_05_051012.pdf?casa_token=0vUaYhkudLcAAAAA:e8XZmLYiYsOaRntV47gJLXGOLwdTkv-n4K4Z8yfJGCYCYSYpeTJ3cJuoMXPHVjwVuDOG8Q by University Of Not

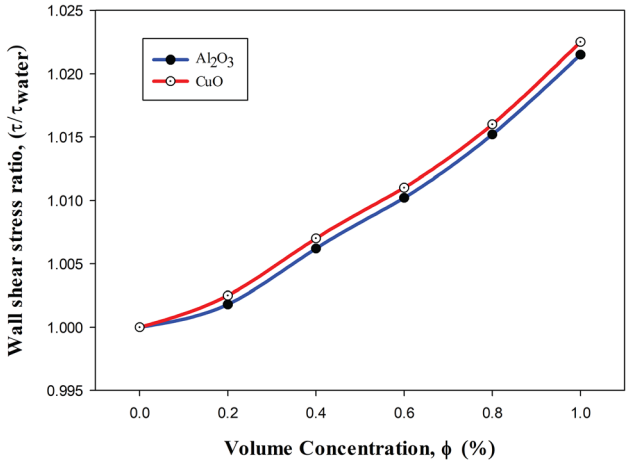


Fig. 14 Variation of average wall shear stress with respect to nanoparticle volume concentration

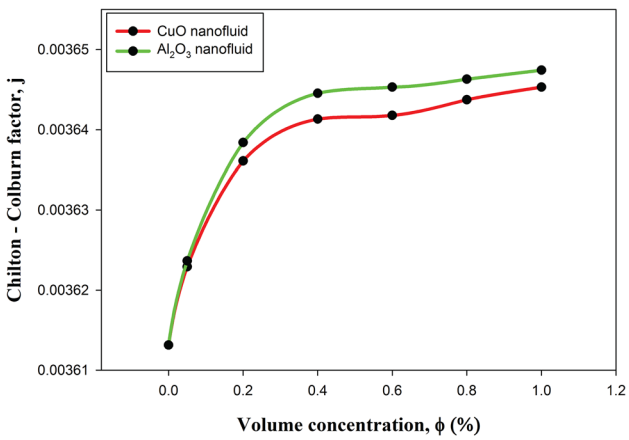


Fig. 15 Variation of Chilton–Colburn factor with respect to nanoparticle volume concentrations for the Reynolds number = 1560

enhancement in convective heat transfer coefficient (h), but the specific heat capacity (C_p) of nanofluid decreases. Enhancement in h is a desirable effect, but the reduction in C_p is an undesirable effect. Reduction in C_p value decreases the heat carrying capacity of fluid. In order to keep the engine at the working temperature, the excess

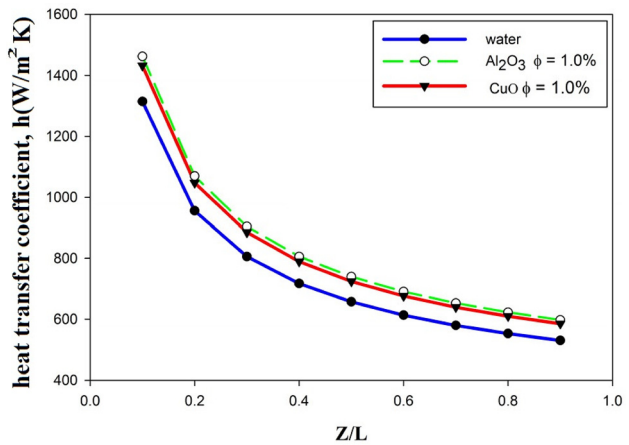


Fig. 16 Variation of convective heat transfer coefficient along the length of the tube for the Reynolds number = 1560

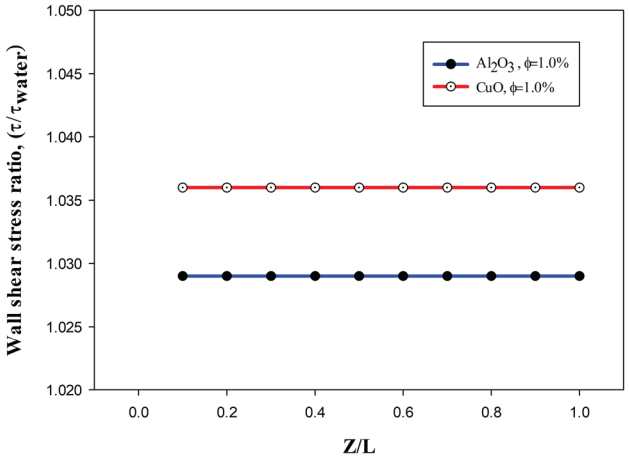


Fig. 17 Variation of wall shear stress along the length of the tube for the Reynolds number = 1560

heat generated should be removed. For the nanofluid with reduced C_p value, the mass flow rate is to be increased, whereas an increment in h improves the ability of the nanofluid to effectively transfer heat at the radiator. In order to quantify the two effects a new term, $h_{ratio} \times C_{p,ratio}$ factor is used. Where convective heat transfer ratio, $h_{ratio} = h_{nanofluid}/h_{water}$ and specific heat capacity ratio, $C_{p,ratio} = C_{p,nanofluid}/C_{p,water}$. The variation of $h_{ratio} \times C_{p,ratio}$ factor with respect to ϕ is plotted in Fig. 20. The factor is more for Al_2O_3/H_2O nanofluid compared to that of Cuo/H_2O nanofluid. For Al_2O_3/H_2O nanofluid, the increment in h is more than that of CuO/H_2O nanofluid and the decrement in C_p is lesser. For both the nanofluids, the factor value is greater than 1 for ϕ value ranges 0–1%, which shows that the desirable effect of increment in h value predominated the undesirable effect of reduction in C_p value.

The convective heat transfer coefficient (h) increases with the increase in specific heat capacity (C_p), thermal conductivity (k), and velocity (V) of the fluid, whereas it reduces with the increase in density (ρ) and viscosity (μ) of the fluid. The addition of nanoparticles increases the k, ρ, and μ however, the C_p value is decreased. The velocity required for the same Reynolds number is lesser for nanofluids compared to that of water. In order to quantify the net effect on the variation in k, C_p, ρ, μ, and V by the addition of nanoparticles, a new factor is defined

$$\text{influence factor} = \frac{k_{ratio} \cdot C_{p,ratio} \cdot V_{ratio}}{\rho_{ratio} \cdot \mu_{ratio}} \tag{36}$$

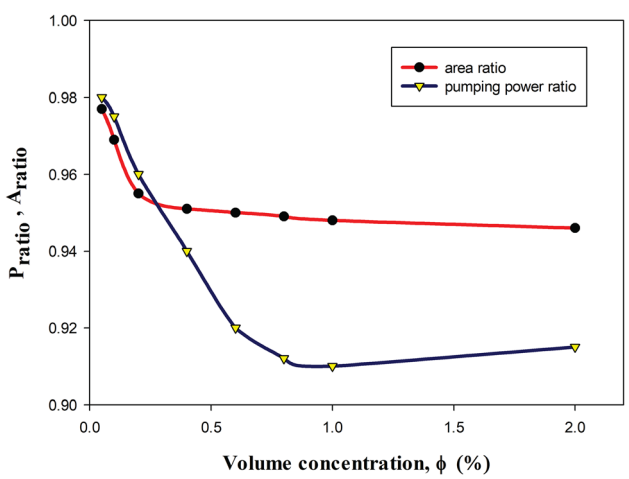


Fig. 18 Variation of pumping power ratio and area ratio for Al_2O_3/H_2O nanofluid for the Reynolds number = 1560

Digitalcollection.asme.org/thermalscienceapplication/article-pdf/10/5/051012/6338855/tsea_010_05_051012.pdf?casa_token=0vUaYhkudLcAAAAA:e8XZmLYiYsOaRntV47gJLXGOLwdTkv-n4K4Z8yfJGCYCYSYpeTJ3cJuoMXPHVjwVuDOG8Q by University Of Not

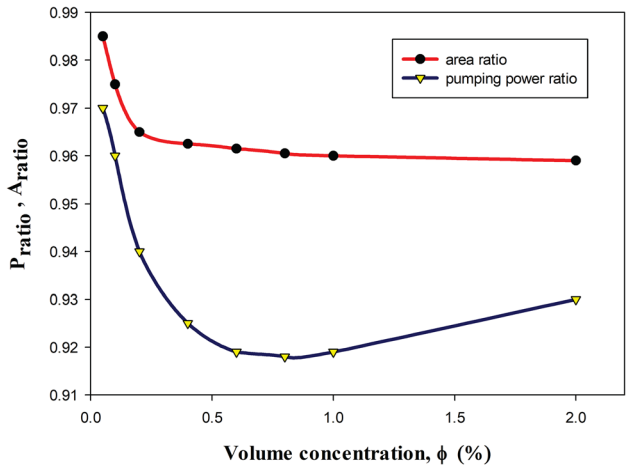


Fig. 19 Variation of pumping power ratio and area ratio for CuO/H_2O nanofluid for the Reynolds number = 1560

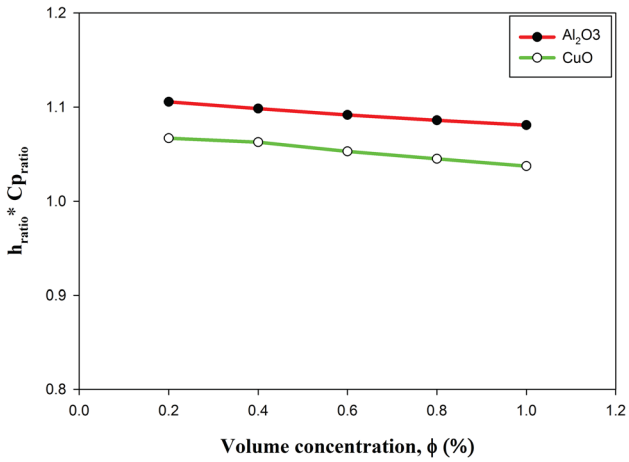


Fig. 20 Variation of $h_{ratio} \times C_{p,ratio}$ factor with respect to nanoparticle volume concentration for the Reynolds number = 1560

where each ratio term corresponds to the fraction of the variable value of the nanofluid to that of base fluid. The variation of influence factor with respect to Reynolds number (Re) for the three fluids are shown in Fig. 21. Since the base fluid in the experimental study is water, its influence factor is 1 for all the Re ranges from 260 to 1560. For the nanofluids, the influence factor is more than 1. Al_2O_3/H_2O nanofluid shows higher influence factor than that of the CuO/H_2O nanofluid. This is the reason for higher convective heat transfer coefficient (h) of Al_2O_3/H_2O nanofluid.

5 Conclusions

Forced convective heat transfer inside a circular tube automobile radiator is investigated using Al_2O_3/H_2O and CuO/H_2O nanofluids. The study was conducted for Reynolds numbers in the range of 260–1560, corresponding to the flow rates of 1–6 l/min.

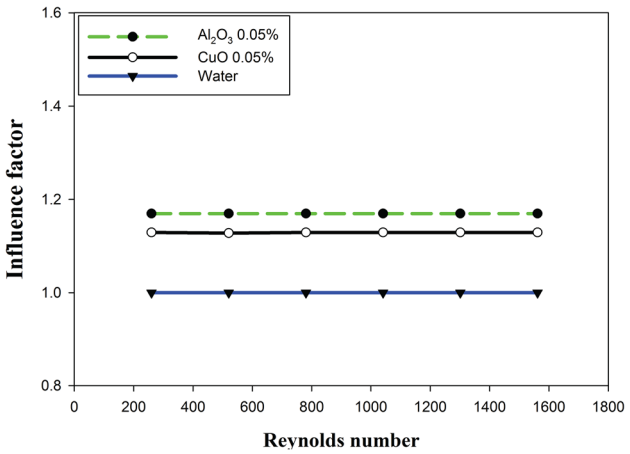


Fig. 21 Variation of influence factor with respect to Reynolds number

The numerical model was validated by using the experimental study results which was conducted with Al_2O_3 and CuO nanofluids with $\phi = 0.05\%$.

Numerical study was conducted for 0–6% nanoparticle concentration (ϕ). The variation in convective heat transfer coefficient (h) was investigated for the ϕ between 0% and 1.0%. The convective heat transfer coefficient h is observed to increase with an increment in Reynolds number (Re) and with the increase in ϕ. It shows a maximum enhancement of 38% and 33% for Al_2O_3 and CuO nanofluids for $\phi = 6.0\%$. Nusselt number (Nu) decreases with ϕ ($0 < \phi < 1.0\%$), and for $\phi > 1.0\%$, Nu is found to increase. The wall shear stress (τ) increases with the increase in ϕ and this enhancement is more for CuO compared to Al_2O_3 nanofluid. A maximum enhancement of 3.0% and 2.5% is obtained for CuO and Al_2O_3 nanofluids for $\phi = 1\%$. The local convective heat transfer coefficient (h_{local}) decreases along the tube length. The h_{local} for a given tube length is higher for Al_2O_3 nanofluid compared to CuO/H_2O nanofluid. A similar trend was noticed in the local wall shear stress (τ_{local}).

Chilton–Colburn factor (j) increases with nanoparticle volume concentration ($0 < \phi < 0.4\%$), though for $\phi > 0.4\%$ the variation is negligible. This is attributed to the fact that frictional losses predominate the enhancement in convective heat transfer. Enhancement in ϕ decreases the pumping power ratio (P_{ratio}). The reduction is observed up to 0.8%. Interestingly the P_{ratio} is then found to increase for higher volume concentrations ($\phi > 0.8\%$).

Addition of nanoparticles enhances the convective heat transfer coefficient (h), whereas it reduces the specific heat carrying capacity (C_p). Increment in the h improves the heat exchanging ability of the fluid with the tube walls, but the reduction in C_p reduces the fluid's capacity to store the heat energy. The factor ($h_{ratio} \times C_{p,ratio}$) includes both these effects and shows a value greater than 1 in both nanofluids for ϕ between 0% and 1%. The factor value is higher for Al_2O_3 nanofluid than CuO nanofluid. The influence factor value of Al_2O_3/H_2O nanofluid remains more than that of CuO/H_2O nanofluid for ϕ between 0% and 1%.

Hence, the higher h for Al_2O_3 nanofluid. Our study shows that the preferred ϕ is between 0.4% and 0.8% for both nanofluids.

Table 3 Comparison of pumping power reduction and area reduction of present work with Ray and coworkers [15]

	Ray and coworkers [15] (Re = 235)		Present study (Re = 1560)	
Fluid	1% Al_2O_3 EG/W	1% CuO EG/W	1% Al_2O_3 water	1% CuO water
Pumping power reduction (%)	4.72	3.01	8.9	7.8
Area reduction (%)	3.73	3.53	5	3.7

Digitalcollection.asme.org/thermalscienceapplication/article-pdf/10/5/051012/6338855/tsea_010_05_051012.pdf?casa_token=0vUaYhkudLcAAAAA:e8XZmLYiYsOaRntV47gJLXGOLwdTkv-n4K4Z8yfJGCYCYSYpeTJ3cJuoMXPHVjwVuDOG8Q by University Of Not

The study also demonstrates that the convective heat transfer performance of Al_2O_3 nanofluid is higher than CuO nanofluid for circular tube radiator.

Acknowledgment

The authors gratefully acknowledge Centre for Engineering Research and Development (CERD), A. P. J. Abdul Kalam Technological University for providing financial support for the present research work.

Funding Data

- Centre for Engineering Research and Development (KTU/CERD/387/2015).

Nomenclature

A = area, m^2
C_p = specific heat capacity, J/kg K
C_r = capacity ratio
d = diameter, m
f = coefficient of friction
h = heat transfer coefficient, W/m^2 K
j = Colburn–Chilton factor
k = thermal conductivity, W/m K
L = length, m
$\dot{m}$ = mass flow rate, kg/s
NTU = number of transfer units
Nu = Nusselt number
P = pressure, N/m^2
Q = heat transfer rate, W
Re = Reynolds number
t = tube wall thickness
T = temperature, K
T_0 = reference temperature, 273 K
U = overall heat transfer coefficient, W/m^2 K
V = velocity, m/s
w = weight, N
W = pumping power, W

Greek Symbols

ε = effectiveness
κ = Boltzmann constant, 1.381×10^{-23} J/K
μ = viscosity, Ns/m^2
ρ = density, kg/m^3
φ = volume fraction
ϕ = volume concentration, %

Subscripts

avg = average
bf = base fluid
hyd = hydraulic diameter
in = inside surface
nf = nanofluid
np = nanoparticle
out = outside surface

References

[1] Choi, S.-S., and Eastman, J., 1995, "Enhancing Thermal Conductivity of Fluids With Nanoparticles," *Developments and Applications of Non-Newtonian Flows* (International Mechanical Engineering Congress and Exposition, Vol. 231), D. A. Siginer and D. A. Siginer, eds., American Society of Mechanical Engineers, New York, pp. 99–105.
[2] Eastman, J., Choi, U., Li, S., Thompson, L., and Lee, S., 1996, "Enhanced Thermal Conductivity Through the Development of Nanofluids," MRS Proc., **457**, p. 3.
[3] Zhu, H. T., Lin, Y. S., and Yin, Y. S., 2004, "A Novel One-Step Chemical Method for Preparation of Copper Nanofluids," J. Colloid Interface Sci., **277**(1), pp. 100–103.
[4] Nguyen, C., Desgranges, F., Roy, G., Galanis, N., Mar, T., Boucher, S., and Mintsa, H. A., 2007, "Temperature and Particle-Size Dependent Viscosity Data for Water-Based Nanofluids Hysteresis Phenomenon," Int. J. Heat Fluid Flow, **28**(6), 1492–1506.
[5] Chavan, D., and Pise, A. T., 2014, "Performance Investigation of an Automotive Car Radiator Operated With Nanofluid as a Coolant," ASME J. Therm. Sci. Eng. Appl., **6**(2), p. 021010.
[6] Bozorgan, N., Krishnakumar, K., and Bozorgan, N., 2012, "Numerical Study on Application of Cuo-Water Nanofluid in Automotive Diesel Engine Radiator," Mod. Mech. Eng., **2**(4), pp. 130–136.
[7] Leong, K., Saidur, R., Kazi, S., and Mamun, A., 2010, "Performance Investigation of an Automotive Car Radiator Operated With Nanofluid-Based Coolants (Nanofluid as a Coolant in a Radiator)," Appl. Therm. Eng., **30**(17–18), pp. 2685–2692.
[8] Vajjha, R. S., and Das, D. K., 2009, "Experimental Determination of Thermal Conductivity of Three Nanofluids and Development of New Correlations," Int. J. Heat Mass Transfer, **52**(21–22), pp. 4675–4682.
[9] Peyghambarzadeh, S., Hashemabadi, S., Hoseini, S., and Jamnani, M. S., 2011, "Experimental Study of Heat Transfer Enhancement Using Water/Ethylene Glycol Based Nanofluids as a New Coolant for Car Radiators," Int. Commun. Heat Mass Transfer, **38**(9), pp. 1283–1290.
[10] Bianco, V., Chiacchio, F., Manca, O., and Nardini, S., 2009, "Numerical Investigation of Nanofluids Forced Convection in Circular Tubes," Appl. Therm. Eng., **29**(17–18), pp. 3632–3642.
[11] Shen, J., Liburdy, J. A., Pence, D. V., and Narayanan, V., 2009, "Droplet Impingement Dynamics: Effect of Surface Temperature During Boiling and Non-Boiling Conditions," J. Phys.: Condens. Matter, **21**(46), p. 464133.
[12] Prasad, P. D., Gupta, A., Sreeramulu, M., Sundar, L. S., Singh, M., and Sousa, A. C., 2015, "Experimental Study of Heat Transfer and Friction Factor of Al_2O_3 Nanofluid in U-Tube Heat Exchanger With Helical Tape Inserts," Exp. Therm. Fluid Sci., **62**, pp. 141–150.
[13] Xuan, Y., and Roetzel, W., 2000, "Conceptions for Heat Transfer Correlation of Nanofluids," Int. J. Heat Mass Transfer, **43**(19), pp. 3701–3707.
[14] Kakaç, S., and Pramuanjaroenkij, A., 2009, "Review of Convective Heat Transfer Enhancement With Nanofluids," Int. J. Heat Mass Transfer, **52**(13–14), pp. 3187–3196.
[15] Ray, D. R., Das, D. K., and Vajjha, R. S., 2014, "Experimental and Numerical Investigations of Nanofluids Performance in a Compact Minichannel Plate Heat Exchanger," Int. J. Heat Mass Transfer, **71**, pp. 732–746.
[16] Maxwell, J. C., 1873, *A Treatise on Electricity and Magnetism*, 1st ed., Vol. 1, Clarendon Press, Oxford, UK.
[17] Einstein, A., 1956, *Investigations on the Theory of the Brownian Movement*, Courier Corporation, Dover publications, Mineola, NY.
[18] Kline, S. J., and McClintock, F., 1953, "Describing Uncertainties in Single-Sample Experiments," Mech. Eng., **75**(1), pp. 3–8.
[19] Maiga, S. E. B., Palm, S. J., Nguyen, C. T., Roy, G., and Galanis, N., 2005, "Heat Transfer Enhancement by Using Nanofluids in Forced Convection Flows," Int. J. Heat Fluid Flow, **26**(4), pp. 530–546.
[20] Heris, S. Z., Esfahany, M. N., and Etemad, S. G., 2007, "Experimental Investigation of Convective Heat Transfer of Al_2O_3/Water Nanofluid in Circular Tube," Int. J. Heat Fluid Flow, **28**(2), pp. 203–210.

gitalcollection.asme.org/thermalscienceapplication/article-pdf/10/5/051012/6338855/tsea_010_05_051012.pdf?casa_token=0vUaYhkudLcAAAAA:e8XZmLYiYsOaRntV47gJLXGOLwdTkv-n4K4Z8yfJGCYCYSYpeTJ3cJuoMXPHVjwVuDOG8Q by University Of Not